

Implementation of Wavelet Encoding Spectroscopic Imaging Technique on a 3 Tesla Whole Body MR Scanner: In vitro Results.

Y. Fu, *Student Member, IEEE*, O. Ijare, G. Thomas, R. Fazel-Rezai, *Senior Member, IEEE*,
and H. Serrai

Abstract— Proton magnetic resonance spectroscopic imaging (MRSI) provides spatial information about tissue metabolite concentrations used in differentiating diseased from normal tissue. Obtaining metabolic maps with high spatial resolution requires long acquisition time where the patient has to lie still inside the magnet bore (scanner) especially if classical Chemical Shift Imaging (CSI) is used. To reduce acquisition time and obtain a more accurate metabolite distribution with low voxel contamination in MRSI, we have recently proposed and successfully implemented a full Wavelet Encoding-Spectroscopic Imaging (WE-SI) technique on a 1.5 Tesla whole body MR clinical scanner. In this paper we describe the implementation of the WE-SI technique at higher magnetic field strength (B_0) on a clinical 3 Tesla Siemens scanner equipped with parallel imaging tools for better sensitivity. This increases the signal to noise ratio (SNR) and allows combination of the proposed technique with the so-called parallel imaging approach for further acquisition time reduction.

I. INTRODUCTION

Magnetic resonance spectroscopic imaging (MRSI) consists of acquiring spatially localized Magnetic Resonance (MR) signals called Free Induction Decay (FID) modeled as a sum of damped sinusoids, and representing the response of spins of different tissue metabolites, experiencing a high homogenous static magnetic field (B_0), to a Radio-Frequency (RF) pulse (B_1 field) transmitted through a coil. MRSI provides a unique modality to non-invasively study tissue metabolism *in vivo* [1]. This technique may provide early prognostic information for better understanding tissue metabolism, differentiating between diseased and normal tissue, improving treatment, reducing risk to the patient [1]. However, acquiring this metabolic information in several spatial dimensions is time consuming, especially if the classical Chemical Shift Imaging (CSI) technique is used [2].

Manuscript received April 6, 2009. This work was supported in part by NSERC-Discovery Grant #RGPIN 327593-06.

Y. Fu is with Institute for Biodiagnostics (IBD), NRC, Winnipeg, MB, Canada and Department of Electrical Engineering, Univ. of Manitoba, Winnipeg, Canada (phone: 204-984-6619 e-mail: yao.fu@nrc-cnrc.gc.ca).

O. Ijare is with Institute for Biodiagnostics (IBD), NRC, Winnipeg, MB, Canada (e-mail: omkar.ijare@nrc-cnrc.gc.ca).

G. Thomas is with Department of Electrical Engineering, Univ. of Manitoba, Winnipeg, Canada (e-mail: thomas@ee.umanitoba.ca).

R. Fazel-Rezai is with Institute for Biodiagnostics (IBD), NRC, Winnipeg, MB, Canada and Department of Electrical Engineering, Univ. of North Dakota, North Dakota, USA. (e-mail: reza@und.edu).

H. Serrai is with Institute for Biodiagnostics (IBD), NRC, Winnipeg, MB, Canada (e-mail: Hacene.Serrai@nrc-cnrc.gc.ca).

To reduce acquisition time, a three dimensional non-Fourier encoding MRSI technique called wavelet encoding-spectroscopic imaging (WE-SI) has been proposed as an alternative to CSI to reduce acquisition time and voxel contamination [3, 4]. In wavelet encoding, a set of dilated and translated prototype functions called wavelets are used to span a localized space by dividing it into a set of sub-spaces with pre-determined sizes and locations. In spectroscopic imaging, this process is achieved using RF pulses with profiles resembling the wavelet shapes. Slice selective excitation and refocusing RF pulses, with single and dual band profiles similar to Haar wavelets, are used in the modified point resolved (PRESS) sequence [5] to acquire three dimensional (3D) WE-SI data. Wavelet dilation and translation are achieved by changing the strength of the localization B_0 field gradients and frequency shift of the RF pulses respectively. The desired spatial resolution in each direction sets the corresponding number of dilations (increases in the localization gradients), and consequently the number of translations (frequency shift) of the Haar wavelets (RF pulses), which are used to collect MR signals from the corresponding sub-spaces. Data acquisition time is reduced by using the minimum recovery time (TR_{min}), necessary for spin relaxation [3, 4], when successive MR signals from adjacent sub-spaces are collected. The inverse wavelet transform is performed on the acquired data to produce metabolite maps. This technique has been implemented and validated on a 1.5 Tesla General Electric (GE) whole body scanner [4]. As compared to CSI, the proposed method is able to reduce acquisition time, while preserving the spatial metabolite distribution. As expected, a decrease in Signal to Noise Ratio (SNR) is noticed in WE-SI data as compared to CSI [4]. To further demonstrate the usefulness of WE-SI and increase its sensitivity, we implemented it at a higher B_0 field using a 3 Tesla Siemens whole body scanner, which is equipped with the so-called parallel imaging tools, where further reduction in acquisition time is expected by combining WE-SI with parallel imaging.

In this paper, we briefly describe the theory of 3D WE-SI, including acquisition time reduction and SNR calculation; we focus on illustrating its implementation on a clinical 3 Tesla Siemens scanner, and show that 3D WE-SI provides accurate results with higher sensitivity while reducing acquisition time and preserving the metabolite spatial information. Finally we propose solutions to increase the SNR, improve data quality, and combine WE-SI technique with parallel imaging for further acquisition time reduction.

II. THEORY

The theory behind the development and implementation of the WE-SI method is discussed in details in [3, 4] and summarized here with a brief description of the SNR and acquisition time calculations. WE-SI is based upon the discrete wavelet transform which uses dilated and translated prototype functions, called wavelets, to perform a linear transformation from a space domain to a wavelet domain. This transform achieves a division of an input finite space function to a set of output sub-spaces with different sizes and locations [6]. The wavelet dilation determines the size of the sub-space while the translation localizes its position. The number of wavelet dilations, which sets the number of translations, is determined by the desired spatial resolution. Similar to the Fourier synthesis, which performs an inverse Fourier transform on the k-space (Fourier domain in MR) data to obtain the input spatial function, an inverse wavelet transform is performed on the sub-spaces (wavelet domain) data to perform the same task [3, 4]. The wavelet dilations and translations are achieved by changing the localization B_0 field gradient strength and by shifting the frequency of the selective RF pulses, respectively. Inverse wavelet transform is achieved on the collected wavelet domain data to obtain metabolite images. Data acquisition time is reduced by shortening the recovery time (TR) to its minimum value (TR_{\min}) in the sequential excitations of pre-determined adjacent sub-spaces [3, 4]. We choose the Haar wavelets as prototype functions due to their implementation simplicity.

Due to the finite support of the wavelet functions, the RF pulses cover a part of the space (sub-space) for each excitation. Thus, if spins are experiencing the RF pulse excitation in a given sub-space, those in the rest of the space are relaxed. By arranging the excitations in an optimal order, a series of these sub-space signals can be acquired without the need of a full TR time [3, 4]. Thus, the total acquisition time required for an acquisition $N_x \times N_y \times N_z$ (defined resolution in three dimensions) is given by:

$$Acq_time = N_x \cdot N_y \cdot N_z \cdot TR - N_{eff} \cdot (TR - TR_{\min}), \text{ where}$$

$$N_{eff} = \left[\begin{array}{l} 2^{2M_x} \cdot (M_x - 2^{M_x} + 6) / 3 + 2^{2M_y+1} \cdot (M_y - 2^{M_y} + 5) / 3 + 2^{M_x+M_y+1} - 2 \cdot 2^{M_x} \\ + 2^{M_x+M_y} \cdot (M_x - 2M_x - 8 + M_x) + 2^{M_y} \cdot (-2M_y + 2 + 2M_x) - 4/3 - P(x) - P(y) \end{array} \right] \dots (1)$$

The following variables are set to: $M_x = \log_2(N_x)$, $M_y = \log_2(N_y)$, $M_z = \log_2(N_z)$, $P(x) = i \cdot 2^{2(i-1)}$, and $P(y) = 2 \cdot j \cdot 2^{2(j-1)}$, where i and j run from 2 to M_x and M_y respectively. If $M_x = M_y = M_z = M$, and $P = P(x) = P(y) / 2$, N_{eff} is simplified to:

$$N_{eff} = N^3 + N^2(3 \log_2(N) - 8) / 3 - 4/3 - 3P.$$

A decrease in SNR occurs in WE-SI at higher resolutions due to the reduction of the size of the excited sub-spaces [6, 7]. As a consequence, the sensitivity in 3D WE-SI compared to Fourier encoding drops by:

$$SNR_{WE-SI} = SNR_{CSI} \sqrt{\frac{27 \cdot N_x \cdot N_y \cdot N_z}{(4 + 2 \cdot N_x^2 + 2 \cdot N_y^2 + N_x^2 \cdot N_y^2) \cdot (N_z^2 + 2)}} \text{, which}$$

$$\text{is approximated to } SNR_{WE-SI} \approx SNR_{CSI} \cdot (3/N)^{3/2} \dots (2)$$

for $N_x = N_y = N_z$.

III. MATERIALS AND METHODS

A. Phantoms and MR acquisition parameters:

The 3D WE-SI scheme is implemented on a 3 Tesla Siemens clinical scanner available at the Institute for Biodiagnostics (IBD-NRC), using Siemens head coil. To assess the performance of the technique in terms of speed and accuracy, we conducted phantom studies at different spatial resolutions. Low resolution $2 \times 2 \times 2$ and $4 \times 4 \times 2$ data are acquired using two home-made phantoms (Fig. 1), and an $8 \times 8 \times 4$ data are acquired using a uniform spherical phantom containing an aqueous solution of brain metabolites with known concentrations. The two home-made phantoms are made from two rectangular plastic holders containing equally spaced 2×2 and 4×4 fourteen mm diameter holes. The size of each phantom is 40 mm \times 40 mm and 70 mm \times 70 mm. Cylindrical tubes filled with aqueous solutions of metabolites with known concentrations are placed in the holes of the plastic holder, dropped in a container filled with water, which in turn immersed in a cylinder filled with canola oil (Fig. 1). The low resolution data are acquired to check the absolute metabolite quantification accuracy and voxel contamination of the method, whereas for the high resolution data, acquisition time and SNR values are calculated. The MR acquisition parameters for all the collected data are: TR=2 sec, echo time (TE) = 75 ms, Acquisition Digital Converter (ADC) bandwidth = 2 kHz, data vector size = 1k points, and four

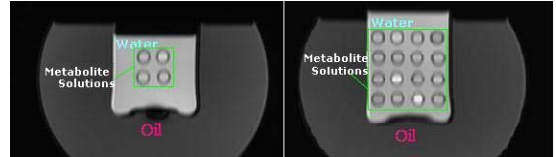


Fig. 1: Localization MR images of the $2 \times 2 \times 2$ (left) and $4 \times 4 \times 2$ (right) phantoms. The box represents the FOV used in the WE-SI sequence.

averages. The field of view (FOV) and slice thickness are 40mm by 40mm, 70mm by 40mm, and 80mm by 80mm for $2 \times 2 \times 2$, $4 \times 4 \times 2$, and $8 \times 8 \times 4$ data sets respectively.

B. Sequence Design:

We have developed the WE-SI technique by modifying the spatially localized PRESS sequence to acquire 3D WE-SI data. Refined sinus cardinal (sinc) functions, representing excitation (90°) and refocusing (180°) RF pulses for the WE-SI sequence, using Shinar-Le Roux algorithm [8] are generated. The profiles of these RF pulses, one single and one dual band resemble scale and Haar wavelet functions respectively (Fig. 2). The excitation RF pulse is applied along the so-called slice direction and the refocusing RF pulses are applied along the so-called phase and read direction by analogy to the imaging sequences [5]. To achieve spatial encoding in the three directions, dilations and translations of the dual band RF pulses as detailed elsewhere [4] are achieved by increasing the selection

gradient strength and shifting the centre frequency of RF pulses respectively. The duration and bandwidth of all RF pulses are 5.2 msec and 2500Hz respectively. Fig. 2 shows the spatial profiles of the RF pulses as executed on the scanner (solid line) versus the Haar wavelet profiles (dashed line), where the difference between the two shapes is in the transition band and the edges. This is mainly due to the short duration of the sinc functions of the RF pulses. The signal loss and cross voxel contamination can be corrected by data reconstruction in the inverse wavelet transform [4].

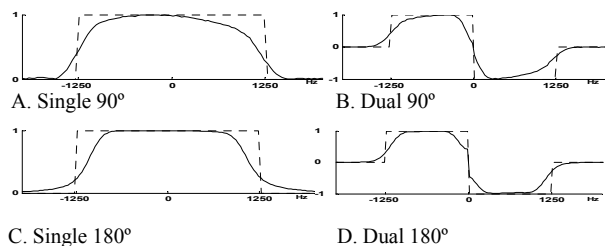


Fig. 2: Profiles of RF pulses (solid lines) used as Haar functions (dashed lines) in the WE-SI sequence.

IV. RESULTS AND DISCUSSION

A. 2×2×2 Phantom Test

WE-SI provides accurate results in term of absolute metabolite quantification. Estimated metabolite concentration values versus the expected ones from the 2×2×2 WE-SI phantom data are given in Table 1. Fig. 3 shows the accurate localization findings of the metabolite peaks along with fitting results (red). Voxel contaminations are insignificant at this low resolution. No acquisition time reduction is obtained at this low resolution, since no wavelet translation (RF pulse shift) is performed [5].

TABLE I
ABSOLUTE ESTIMATION OF METABOLITE CONCENTRATIONS IN MILLI-MOLAR (mM) FOR 2×2×2 PHANTOM

metabolite \ voxel		voxel			
		NAA	Creatine	Choline	Water
NAA (mM)	estimated	144.3	0	0	0
	expected	150	0	0	0
Creatine (mM)	estimated	0	64.5	3.7	0
	expected	0	65	0	0
Choline (mM)	estimated	0	0	48.1	0
	expected	0	0	50	0

TABLE II
THEORETICAL AND EXPERIMENTAL ACQUISITION TIMES

Resolution	Total Acquisition Time		
	Experiment	Calculated	reference (CSI)
2×2×2	32 sec	32 sec	32 sec
4×4×2	3min 16 sec	3 min 11sec	4min 16sec
8×8×4	20min 24sec	20min 50sec	34min 28sec

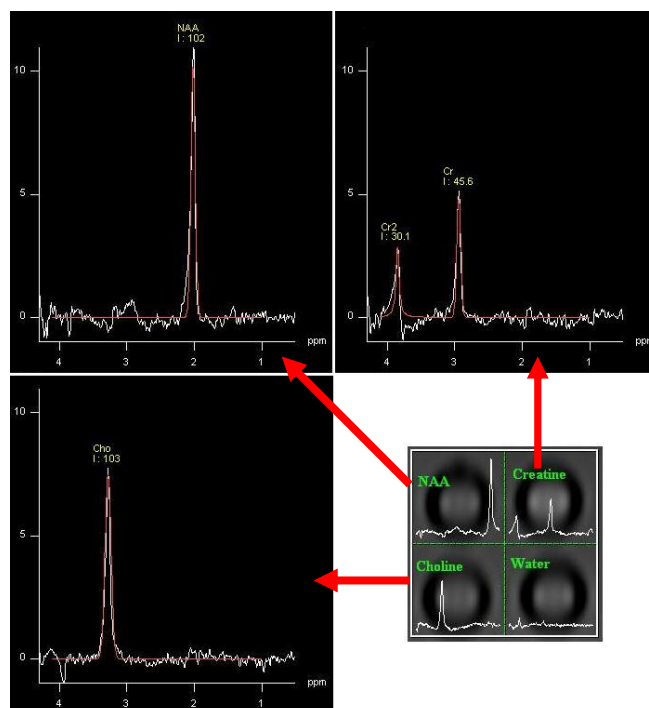


Fig. 3: Front axial slice of acquired metabolite spectra for the 2×2×2 WE-SI data and fitting results (red). The area under the peak is evaluated and displayed as 1; absolute concentration is calculated using a reference with known concentration.

B. 4×4×2 Phantom Test

Acquisition time reduction of 23.4% as compared to CSI time is obtained at this resolution (Table II). The experimental results are consistent with the theoretical ones (Eq. 1). The results also show that WE-SI preserves the metabolite spatial localizations with low voxel contamination (Table III, Fig. 4). Voxel contamination is calculated by dividing the area of any metabolite peak detected in any voxel by its area in the expected voxel. In voxel-(1, 3) for example, only Choline peak is expected. However, small contamination from N-Acetyl-Aspartate (NAA) peak, from adjacent voxel-(2, 3) is observed (Fig. 4). The contamination is calculated by dividing the area of NAA peak in voxel-(1, 3) to the area of the NAA peak from voxel-(2, 3).

Voxel contamination in WE-SI at 3 Tesla is mainly due to the RF profiles not perfectly matching the shapes of the Haar functions (Fig. 2). The tails of the RF pulse profiles in solid lines in Fig. 2 extends outside the boxcar shown in dashed line. These tails pick up a small portion of signal from neighboring voxels. In addition the transition bands are large causing voxel contamination. To minimize the profile errors, we replaced the Haar function values (1 and -1) in the inverse wavelet transform by numbers obtained from the fit of the RF pulse profiles to boxcar shapes [4]. Another reason for voxel contamination is the B_0 field inhomogeneity. At higher B_0 field strength, homogeneity is more difficult to achieve, especially with phantoms made from glass vials, plastic holders and containers, which complicates more the shimming process for better B_0 field

homogeneity due to susceptibility magnetic field effects [9]. As shown in Fig. 4, we observe more contaminations in the bottom row, because of the poor shimming at that location.

TABLE III
CONTAMINATION EVALUATION FOR THR 4×4×2 PHANTOM

Voxel	Main Metabolites	Contamination
(1, 1)	None (water)	0
(2, 1)	Acetone	0
(3, 1)	Sarcosine	0
(4, 1)	Glycine	Succinate (6.27 %)
(1, 2)	NAA	0
(2, 2)	None (water)	0
(2, 3)	Creatine	0
(2, 4)	Succinate	0
(1, 3)	Choline	NAA (2.33%)
(2, 3)	NAA	0
(3, 3)	Choline	NAA (4.74%)
(4, 3)	Sarcosine	Choline (4.51%) Acetone (12.72%)
(1, 4)	Glycine	0
(2, 4)	Creatine	NAA (9.3%)
(3, 4)	NAA	0
(4, 4)	Acetone	Succinate (5.26%)

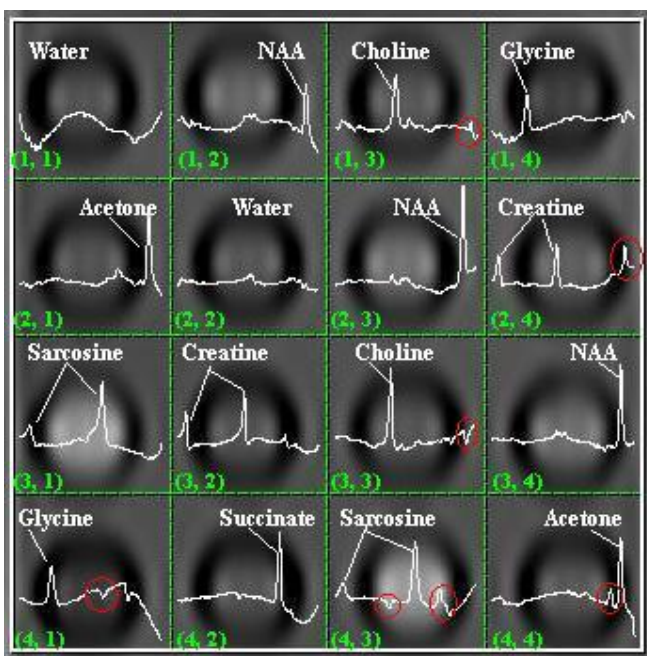


Fig. 4: Front axial slice of acquired metabolite spectra for the 4×4×2 WE-SI and voxel contaminations in red circles.

C. 8x8x4 Spherical Phantom Test

This test is performed to evaluate and compare the SNR of the WE-SI versus the CSI. As expected the SNR measured from a subset of voxels located at the center of the sphere (B_0 field is homogenous at the center of the sphere) is lower by 28.8% as compared to CSI. These results are comparable to the calculated ones at 29.9% (Eq. 2). Better sensitivity is obtained at higher field (3 Tesla), than lower field (1.5 Tesla) [10]. Acquisition time reduction is also obtained at this resolution (Table II).

V. CONCLUSION

A three dimensional wavelet encoding method for acquiring magnetic resonance spectroscopic imaging data is presented. The proposed WE-SI is compared to the gold standard CSI technique. This comparison, offers a valuable indication of acquisition time, voxel contamination and sensitivity. Previous results [4] along with the results shown here demonstrate that compared to the CSI method, wavelet encoding technique is able to reduce acquisition time while preserving the spatial distribution of metabolites. The reduction in acquisition time is directly proportional to the spatial resolution and dimensions. Voxel contamination in WE-SI is independent from spatial resolution [11]. Although the SNR of WE-SI is lower than CSI, results obtained at 3 Tesla are better in sensitivity than those obtained at 1.5 Tesla [10]. In order to increase the SNR, less spatially localized wavelets should be used [7, 11]. To reduce data reconstruction artifacts, which are the main sources of voxel contamination, wavelets with smoother decay and shorter duration that are less dependent on the profiles of the RF pulses should be tested [7]. As a consequence, shorter RF pulses could be used and data with shorter echo times could be acquired, which increase data sensitivity [4]. To further reduce acquisition time, WE-SI technique is being combined with the parallel imaging approach [12].

Acknowledgment

Sponsored by NSERC-Discovery Grant #RGPIN 327593-06

REFERENCES:

- [1] Gruber, S.; Stadlbauer, A.; Mlynarik, V.; Gatterbauer, B.; Roessler, K.; Moser, E., "Proton magnetic resonance spectroscopic imaging in brain tumor diagnosis", *Neurosurgery Clinics of North America*, 2005, 16, (1), 101-114.
- [2] Brown, T. R.; Kincaid, B. M.; Ugurbil, K., "NMR chemical shift imaging in three dimensions", *Proceedings of the National Academy of Sciences*, 1982, 79, 3523-3526.
- [3] Serrai, H.; Senhadji, L., "Acquisition time reduction in magnetic resonance spectroscopic imaging using discrete wavelet encoding", *Journal of Magnetic Resonance*, 2005, 177, (1), 22-30.
- [4] Young, R.; Serrai, H., "Implementation of three-dimensional wavelet encoding spectroscopic imaging: In vivo application and method comparison", *Magnetic Resonance in Medicine*, 2009, 61, (1), 6-15.
- [5] Bottomley, P. A., "Selective volume method for performing localized NMR spectroscopy", US patent N°4 -480-226, 1984.
- [6] Daubechies, I., *Ten Lectures on Wavelets*. In CBMS-NSF Lectures, Society for Industrial and Applied Mathematics (SIAM): 1992, SIAM-61.
- [7] Weaver, J.; Healy, D., "Signal-to-noise ratios and effective repetition times for wavelet encoding and encoding with wavelet packet bases", *Journal of Magnetic Resonance (A)*, 1995, 113, 1-10.
- [8] Cunningham, C. H.; Wood, M. L., "Method for improved multiband excitation profiles using the Shinnar-Le Roux transform", *Magnetic Resonance in Medicine*, 1999, 42, (3), 577-584.
- [9] Yablonsky, D. A.; Haacke, E. M., "Theory of NMR signal behavior in magnetically inhomogeneous tissues: the static dephasing regime", *Magnetic Resonance in Medicine*, 1994, 32, (6), 749-763.
- [10] Haacke, E. M., In "Magnetic Resonance Imaging", Wiley, Eds. 1999.
- [11] Panych, L. P., "Theoretical comparison of Fourier and wavelet encoding in magnetic resonance imaging", *IEEE Transactions on Medical Imaging*, 1996, 15, (2), 141-153.
- [12] Fu, Y.; Serrai, H. "High speed magnetic resonance spectroscopic imaging using wavelet encoding and parallel imaging", *Proc. Intl. Soc. Mag. Reson. Med.*, 2008, 15, 1582.